How C-Terminal Carboxyamidation Alters the Biological Activity of Peptides from the Venom of the Eumenine Solitary Wasp[†]

Maurício L. Sforça,[‡,§] Sérgio Oyama, Jr.,[‡,§] Fernanda Canduri,[∥,⊥] Carla C. B. Lorenzi,[∥,⊥] Thelma A. Pertinhez,[‡] Katsuhiro Konno,[∥,@] Bibiana M. Souza,[∥,@] Mário S. Palma,[∥,@] J. Ruggiero Neto,[∥,⊥] Walter F. Azevedo, Jr.,[∥,⊥] and Alberto Spisni*,[‡,#]

Center for Structural Molecular Biology, BioNMR Laboratory, LNLS, Campinas, SP, Brazil, Center of Study of Social Insects, Department of Biology, Institute of Biosciences, UNESP, Rio Claro, SP, Brazil, Center for Applied Toxicology-CEPID-FAPESP, Institute Butantan, São Paulo, SP, Brazil, Department of Physics, IBILCE, UNESP, São José do Rio Preto, SP, Brazil, and Department of Experimental Medicine, Section of Chemistry and Structural Biochemistry, University of Parma, Parma, Italy

Received November 21, 2003; Revised Manuscript Received March 15, 2004

ABSTRACT: Inflammatory peptides display different types of post-transcriptional modifications, such as C-terminal amidation, that alter their biological activity. Here we describe the structural and molecular dynamics features of the mast cell degranulating peptide, eumenine mastoparan-AF (EMP-AF-NH$_2$), found in the venom of the solitary wasp, and of its carboxyl-free C-terminal form (EMP-AF-COO$^-$) characterized by a reduced activity. Circular dichroism indicates that both peptides switch from a random coil conformation in water to a helical structure in TFE and SDS micelles. NMR data, in 30% TFE, reveal that the two peptides fold into an α-helix spanning most of their length, while they differ in terms of molecular rigidity. To understand the origins of the conformational flexibility observed in the case of EMP-AF-COO$^-$, a 5 ns MD simulation was carried out for each peptide, in an explicit water/TFE environment. The results show that the two peptides differ in an H-bond between Leu14 NH$_2$ and the backbone carbonyl of Ile11. The loss of that H-bond in EMP-AF-COO$^-$ leads to a significant modification of its structural dynamics. In fact, as evidenced by essential dynamics analysis, while EMP-AF-NH$_2$ exists mainly as a rigid structure, EMP-AF-COO$^-$ presents two helical stretches that fluctuate in some sort of independent fashion. We conclude that the diverse biological activity of the two peptides is not simply due to the reduction of the net positive charge, as generally suggested, but also to a structural perturbation of the amphipathic α-helix that affects their ability to perturb the cell membrane.

The insects of the order Hymenoptera are classified into two groups, based on their life history: social and solitary. The venom of social Hymenoptera evolved for use as a defensive tool to protect the colonies of honeybees and wasps from the attacks of predators. Small peptides are one of the major components of these venoms and include melittin and mast cell degranulating (MCD)[1] peptides in honeybees, while mastoparans and chemotactic peptides are present in social wasps. On the other hand, solitary hymenopteran venoms evolved for use as a tool for paralyzing and/or killing prey. Therefore, the major components of these venoms are neurotoxins, though they also contain MCD peptides. These last ones possess structures closely related to mastoparans from social wasps, presenting amphipathic helical structure and exhibiting similar degranulating activity. These peptides have been characterized both chemically and pharmacologically (1−3). Their potent degranulation, hemolytic, and antimicrobial activity has been ascribed to their ability to interact with the cell membrane surface via the positively charged side of their amphipathic α-helical structure.

Frequently, the biological activity of these peptides is associated with some type of post-transcriptional processing of their precursors, such as C-terminal amidation. This occurs in melittin (4), cecropins (5), dermaseptins (6), PGLa (7), clavanin (8), PR-39 (9), apidaecins (10), diptericin (11), polyphemusins (12), or penaeidins (13). There are also studies showing an increase in activity following amidation or, alternatively, an activity decrease when the amide is removed (14−16).

* To whom correspondence should be addressed: CeBiME, Laboratório Nacional de Luz Síncrotron, C.P. 6192, CEP 13084-971, Campinas, SP, Brazil; fax, +55 19 32877110; e-mail, alberto@lnls.br; or Department of Experimental Medicine, University of Parma, Parma, Italy; fax, +39 0521 903802; e-mail, aspin@unipr.it.
  [‡] CeBiME-LNLS.
  [§] These authors contributed equally to this work.
  [∥] CAT, Institute Butantan.
  [⊥] Department of Physics, IBILCE, UNESP.
  [@] Center of Study of Social Insects, Institute of Biosciences, UNESP.
  [#] Department of Experimental Medicine, University of Parma.

[1] Abbreviations: CD, circular dichroism; DQF-COSY, double-quantum-filtered correlation spectroscopy; ED, essential dynamics; ESI-MS, electrospray ionization mass spectrometry; MCD, mast cell degranulating; MD, molecular dynamics; NMR, nuclear magnetic resonance; NOESY, nuclear Overhauser enhancement spectroscopy; rmsd, root-mean-square deviation; rmsf, root-mean-square fluctuation; SDS, sodium dodecyl sulfate; TFE, 2,2,2-trifluoroethanol; TOCSY, total correlation spectroscopy.

Though the precise mechanism of action of these peptides is not known yet, it is believed they target the lipid component of cell membranes, disrupting the membrane structure via either the "barrel stave mechanism" or the "carpet-like mechanism" (*17−19*).

Recently, a new inflammatory peptide presenting mast cell degranulating activity, eumenine mastoparan-AF (INLLKIAKGIIKSL-NH$_2$, EMP-AF-NH$_2$), has been isolated from the venom of the solitary wasp *Anterhynchium flavormarginatum micado* (*20−22*). The same authors also showed that EMP-AF-NH$_2$ has a more potent biological activity than its analogue containing a carboxyl-free C-terminus, INLLKIAKGIIKSL-COO$^-$ (EMP-AF-COO$^-$; *20*).

Recognizing that the biological activity of these cytolytic peptides may be strongly influenced by the conformation they acquire before interacting with the membranes (*23, 24*), we have decided to study the conformational features of these peptides at that specific stage. To mimic such a unique chemical environment, characterized by a dielectric constant reduced compared to that of bulk water, we have carried out these studies in a H$_2$O/TFE mixture (*24−26*). In this work, we focus on the description of the possible structural differences that we believe lead to the diverse biological activity of these two peptides. The NMR-derived solution structures of EMP-AF-NH$_2$ and EMP-AF-COO$^-$ indicate that the removal of the C-terminal NH$_2$ group induces a localized destabilization of the extended α-helical organization that characterizes the amidated form. To disclose the origin of that structural instability, we carried out 5 ns molecular dynamics (MD) simulations in an explicit water/TFE environment for both peptides. On the basis of ED analysis, a mechanistic model that justifies their structural and functional features is presented.

MATERIALS AND METHODS

Chemicals. 2,2,2-Trifluoroethanol (TFE) was purchased from Aldrich Inc. Perdeuterated 2,2,2-trifluoroethanol (TFE-d_3) was purchased from Cambridge Isotopes Laboratories. Sodium dodecyl sulfate (SDS) was purchased from Pharmacia Fine Chemicals.

Peptide Synthesis and Purification. The peptides were prepared by stepwise manual solid-phase synthesis using *N*-9-fluorophenylmethoxycarbonyl (Fmoc) chemistry with Novasyn TGS resin (NovaBiochem). Side chain protective groups included *tert*-butyl for serine and *tert*-butoxycarbonyl for lysine. Cleavage of the peptide−resin complex was performed by treatment with a trifluoroacetic acid/1,2-ethanedithiol/anisole/phenol/water mixture (82.5:2.5:5:5:5 by volume), using 10 mL per gram of complex at room temperature over the course of 2 h. After being filtered to remove the resin, the crude peptides were extracted with ethyl ether and purified using a semipreparative reversed-phase HPLC column (Shiseido C18, 250 mm × 10 mm), under isocratic conditions, with a 40% (v/v) acetonitrile/water mixture containing 0.1% (v/v) trifluoroacetic acid. The homogeneity and correct sequence of the synthetic peptides were assessed by Edman degradation chemistry, analytical HPLC, and ESI-MS analysis.

Peptide Concentration. Because of the absence of any aromatic residue, the peptide concentration was determined by quantitative amino acid analysis.

CD Spectroscopy. Circular dichroism (CD) experiments were carried out using a Jasco 810 spectropolarimeter (JASCO International Co. Ltd.), coupled to a Peltier Jasco PFD-425S system for temperature control. The peptide samples were dissolved either in a TFE/H$_2$O solvent mixture, with a variable solvent ratio as indicated in the text, or in the presence of SDS micelles (8 mM SDS, pH 4.5) to yield a final peptide concentration of 50 μM for both EMP-AF-NH$_2$ and EMP-AF-COO$^-$. Spectra were collected from 195 to 250 nm and averaged over four scans at 20 °C, with a quartz cell with a path length of 1 mm. A 0.5 nm step resolution, a 50 nm/min speed, an 8 s response time, and a 1 nm bandwidth were generally used. Following baseline correction, the observed ellipticity θ (millidegrees) was converted to the molar mean residue ellipticity [θ] (degrees per square centimeter per decimole). The peptide helical content was estimated according to the method of Chen et al. (*27*).

NMR Spectroscopy. The samples for NMR measurements were prepared by dissolving the peptides in a TFE-d_3/H$_2$O mixture (30:70, v/v) at pH 4.5 to yield a concentration of 1.0 mM for both EMP-AF-NH$_2$ and EMP-AF-COO$^-$. ^{1}H NMR experiments were carried out on a Varian Inova 500AS spectrometer (Varian, Inc.) operating at 499.730 MHz for the ^{1}H frequency and at 20 °C. The proton chemical shifts were referenced to 4,4-dimethyl-4-silapentane-1-sulfonate (DSS, 0.00 ppm). To assign the peptide resonance peaks, standard methods were used, including double-quantum-filtered (DQF)-COSY (*28*), total correlation spectroscopy (TOCSY) using a DIPSI spin-lock sequence and a field strength of 10 kHz (*29*), and nuclear Overhauser enhancement spectroscopy (NOESY) (*30, 31*) experiments. NOESY spectra with mixing times of 100, 200, and 300 ms were recorded to check for spin diffusion. All two-dimensional experiments were carried out in the phase-sensitive mode using the States method (*32*). The spectral width was typically 6000 Hz, and 512 τ_1 increments with 32 transients of 1024 complex points for each free induction decay were recorded. In the case of the DQF-COSY experiments, 1024 τ_1 increments were collected each with 32 transients of 4096 complex points. Water suppression was achieved by low-power continuous wave irradiation during the relaxation delay or WET pulse technique.

Data were processed on a Silicon Graphics Octane 2 workstation using FELIX NMR 2000 (Accelrys Inc.) and nmrPIPE/nmrVIEW (*33, 34*). Prior to Fourier transformation, the time domain data were zero-filled in both dimensions to yield a 4K × 2K data matrix. When necessary, a fifth-order polynomial baseline correction was applied after transformation and phasing. The DQF-COSY experiment was processed to a 16K × 2K data matrix to obtain 0.36 Hz/point of digital resolution for coupling constant measurements.

To obtain interproton distance constraints, the cross-peak volumes of the 300 ms NOESY spectra were measured and calibrated with respect to the cross-peak volume of geminal β-protons, corresponding to an interproton distance of 1.8 Å. The obtained NOE values were classified as strong, medium, and weak, corresponding to upper bound distances of 2.8, 3.5, and 4.0 Å, respectively. The lower bound was taken to be the sum of the van der Waals radii (1.8 Å) for the interacting protons.

Molecular Modeling. The NMR-derived solution structures of EMP-AF-NH$_2$ and EMP-AF-COO$^-$ were computed using the simulated annealing methods in the DYANA (*35*) refine module. The modeling protocol was based on the methods implemented by Pristovšek et al. (*36*). Each round of refinement started with 20 random conformers, and the 10 models with the lowest target function were used to analyze constraint violations and assign additional NOE constraints to be included in the subsequent calculation. This process was repeated until all NOEs had been inserted and all violations eliminated. In the final round of refinement, a total of 100 structures were calculated, and the 40 conformers with the lowest target function (0.41 ± 0.02 Å^2 for EMP-AF-NH$_2$ and 0.29 ± 0.01 Å^2 for EMP-AF-COO$^-$) were considered for analysis. After simulated annealing had been carried out, these 40 structures, with no distance violation larger than 0.2 Å and no dihedral angle violation grater than 5°, were energy minimized with a full consistent valence force field (*37, 38*) by steepest descents and conjugated gradients using several thousand interactions until the maximum derivative was less than 0.001 kcal/Å. All calculations were carried out on an Octane2 workstation (Silicon Graphics Inc.) using the DISCOVER (Accelrys Inc.) software package, together with INSIGHTII as the graphic interface. The quality of the final structures was analyzed using PROCHECK-NMR (*39*) and CNS (*40*).

MD Simulations. The MD calculations and trajectory analysis were performed using the GROMACS suite of programs (*41*) running on a Compaq AlphaServer ES40 multiprocessor. Molecular visualization procedures were carried out using the INSIGHTII graphical environment on an Octane2 workstation.

(1) System Setup. The initial structures were immersed in a triclinic box filled with a mixture of simple point charge (SPC) water molecules (*42*) and TFE model (*43*) molecules, corresponding to an approximately 30:70 (v/v) TFE/H$_2$O mixture. The resulting systems were composed by 67 TFE and 800 H$_2$O molecules for EMP-AF-NH$_2$ and 64 TFE and 804 H$_2$O molecules for EMP-AF-COO$^-$. Each box size was adjusted to ensure a minimum distance of 0.8 nm between the peptide and the periodic box edges. The N-terminus was treated as charged ammonium, and in the case of the carboxyl-free peptide, the C-terminus was treated as a carboxylate group. The net charges of the peptides (+4 for EMP-AF-NH$_2$ and +3 for EMP-AF-COO$^-$) were neutralized with a corresponding number of Cl$^-$ counterions.

(2) Simulation Parameters. The calculations were performed using the GROMACS all-hydrogen force field. The systems were simulated using periodic boundary conditions with a cutoff radius of 0.8 nm for short-range interactions and updating the neighbor pair list every 10 steps. Long-range electrostatic interactions were treated with the Particle Mesh Ewald method (*44, 45*). The LINCS algorithm (*46*) was used to constrain all bond lengths and SETTLE (*47*) to constrain water geometries. A time step of 2 fs was chosen for integrating the equations of motion. The simulations were performed at a constant temperature (293 K) and pressure (1 bar).

(3) Simulation Protocol. A canonical α-helix conformation was used as a starting model for both EMP-AF-NH$_2$ and EMP-AF-COO$^-$ peptides. The solvated peptides were submitted to an initial relaxation of solvent and ions through 500 steps of the steepest descents algorithm while keeping the peptide backbone coordinates fixed. After the constraints had been removed, the systems were submitted to another short minimization step and the molecular dynamics simulations proceeded without any restraint for 5 ns. The atomic positions were recorded every 1.0 ps throughout each trajectory.

ED Analysis. ED was used to obtain a quantitative characterization of the dynamic properties of each system (*48*). The covariance matrices describing the positional fluctuations of the Cα atoms were diagonalized, resulting in sets of eigenvectors and corresponding eigenvalues. The eigenvectors indicate directions in a 3*N*-dimensional space (where *N* is the number of atoms) where there are concerted fluctuations of the atoms. The eigenvalues are equivalent to the total mean square displacement of the atoms along their corresponding eigenvectors. Concerted intramolecular motions within the subspace can be studied by projecting the trajectory onto the individual eigenvectors.

RESULTS

CD Spectroscopy. As shown in panels a and b of Figure 1, the two peptides present a random conformation in water, while they acquire a helical conformation at a TFE concentration higher than 15%. The insets of panels a and b of Figure 1 show that the increase in the helical content, as judged by the intensity of the 222 nm band (*27*), reaches its maximum at ∼30% TFE and can be estimated to be 62% for EMP-AF-NH$_2$ and 29% for EMP-AF-COO$^-$.

Figure 1c shows the CD spectra of both peptides in the presence of 8 mM SDS. Also in this case, the peptides acquire an α-helical configuration. However, comparing the CD spectra of the peptides in 40% TFE with those in the presence of 8 mM SDS, we observe that, in the case of EMP-AF-NH$_2$, in SDS micelles there is a net increase in the optical activity that, combined with the shift of the negative band from 206 to 208 nm, suggests that the peptide acquires a higher α-helical content (83%). As for EMP-AF-COO$^-$, on the other hand, not many differences are observed. In fact, the calculation of the helical content gives a value of 31%.

NMR Spectroscopy. Sequential resonance assignments of EMP-AF-NH$_2$ and EMP-AF-COO$^-$ in a 30:70 (v/v) TFE/H$_2$O mixture has been performed on the basis of the combined use of two-dimensional TOCSY and NOESY experiments (*49*).

The proton chemical shifts of the two peptides together with the $^3J_{NH\alpha}$ coupling constants, estimated from the antiphase cross-peak in the DQF-COSY experiment, have been deposited in the BioMagResBank (BMRB) database as entries 5883 (EMP-AF-NH$_2$) and 5916 (EMP-AF-COO$^-$).

Figure 2 displays the plot of the α-proton chemical shifts index (CSI; *50*) for the two peptides. In the case of EMP-AF-NH$_2$, the negative values observed from residue Leu3 to Leu14, together with the $^3J_{NH\alpha}$ coupling constant of <6.0 Hz for almost all residues, suggest the existence of a helical segment extending over that region. As for EMP-AF-COO$^-$, the data suggest the presence of an α-helical conformation in the Leu3−Lys8 region. However, the smaller α-proton Δδ values coupled with the slightly higher $^3J_{NH\alpha}$ indicate the existence of a less stable helical conformation.
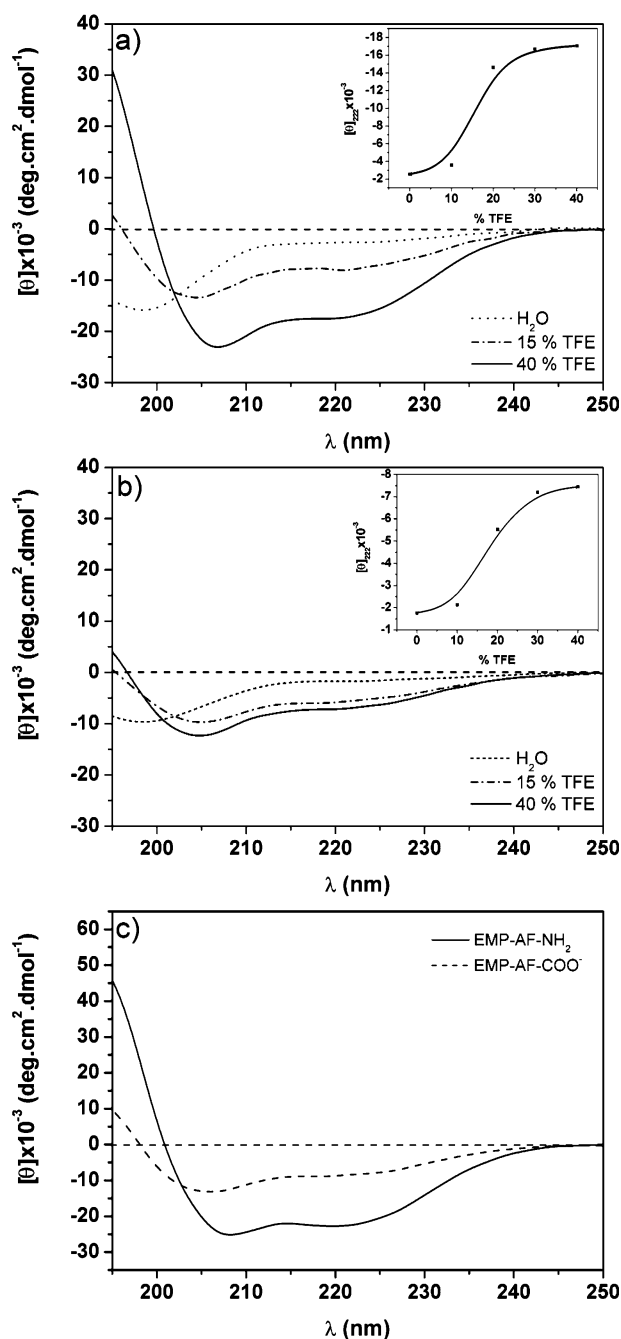
FIGURE 1: TFE titration in the CD far-UV region for (a) EMP-AF-NH$_2$ and (b) EMP-AF-COO$^-$. The insets give the molar ellipticity at 222 nm ($[\theta]_{222}$) as a function of TFE concentration. (c) CD spectra in the far-UV region of EMP-AF-NH$_2$ and EMP-AF-COO$^-$ in the presence of 8 mM SDS. The peptides were dissolved at a final concentration of 50 μM, at pH 4.5. Measurements were carried out at 20 °C.

FIGURE 2: H$_\alpha$ proton chemical shifts index of (a) EMP-AF-NH$_2$ and (b) EMP-AF-COO$^-$, in a 30:70 (v/v) TFE/H$_2$O mixture, at 20 °C. The chemical shift differences were calculated by subtracting the experimental values from the random coil shifts reported in the literature (*50*).

The pattern of inter-residue NOEs for the two peptides is reported in Figure 3, and it shows a good correlation with the CSI values. In fact, the medium-range $d_{\alpha\beta}(i, i + 3)$, $d_{\alpha N}(i, i + 3)$, and $d_{\alpha N}(i, i + 4)$ NOEs together with the intense $d_{NN}(i, i + 1)$ indicate an α-helical fold spanning residues 3−14 for EMP-AF-NH$_2$. In the case of EMP-AF-COO$^-$, though overall the NOEs are consistent with a helical conformation extending over the same region, the smaller number or absence of $d_{\alpha\beta}(i, i + 3)$, $d_{\alpha N}(i, i + 3)$, and $d_{\alpha N}(i, i + 4)$ from residue 9 to 14 confirms the presence of a less stable helical conformation in the C-terminus.
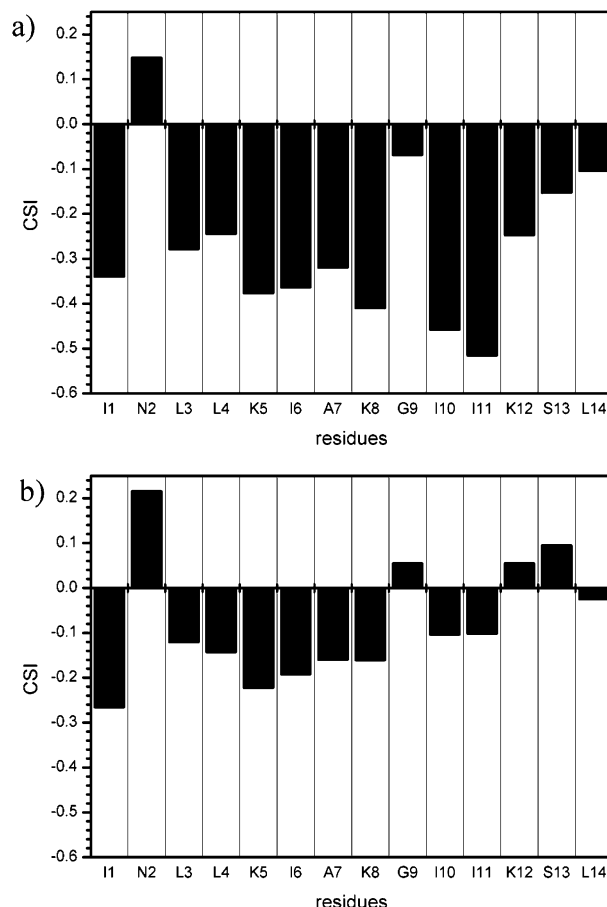
Molecular Modeling. A total of 180 distance constraints, of which 36 are medium-range, for EMP-AF-NH$_2$ and 210 distance constraints, including 24 medium-range, for EMP-AF-COO$^-$ were used for structure calculation using DYANA (*35*).

Figure 4a is the superposition of the 20 minimum energy structures of EMP-AF-NH$_2$. The models have been superimposed in the region of residues 3−14 and show that the peptide folds into a very well-defined amphipathic α-helix. A quite different situation is encountered in the case of EMP-AF-COO$^-$. In fact, the analysis of the NMR-derived structures reveals the existence of various conformational families. Figure 4b shows that a total of 35 minimum energy structures present a well-defined helical stretch spanning residues 3−8. On the other hand, an analysis of the peptide C-terminus allows identification of four main structural families where residues 9−14 give rise to discrete helical conformations. Overall, the peptide appears to be characterized by a significant degree of molecular plasticity that results in a clear structural fluctuation.

The structural statistics are summarized in Table 1, and they show no significant violation of the distance restraints, indicating a good correspondence between the experimental NOEs and the calculated models. PROCHECK-NMR (*39*) has been used to evaluate the quality of the energy-minimized structures. As can be seen in Table 1, the backbone rmsd for all residues is 0.26 ± 0.13 Å for EMP-AF-NH$_2$ and
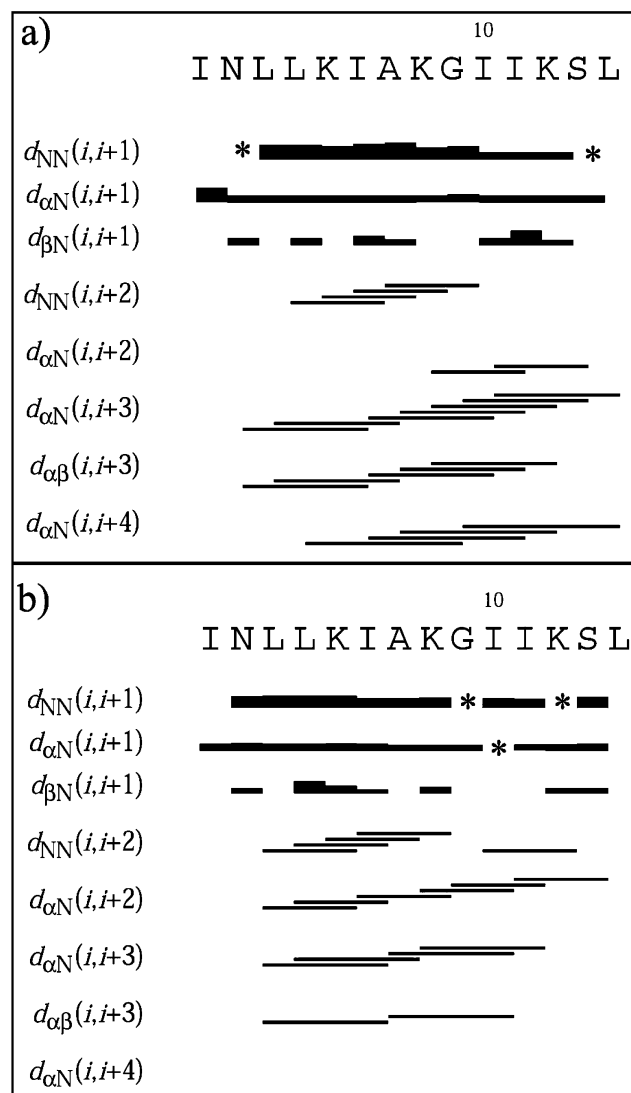
a)

b)

FIGURE 3: Summary of the sequential and medium-range NOE connectivities for (a) EMP-AF-NH$_2$ and (b) EMP-AF-COO$^-$ in a 30:70 (v/v) TFE/H$_2$O mixture, at 20 °C and pH 4.5. The intensities of the experimental NOEs are represented by the thickness of the lines and are classified as strong, medium, and weak, corresponding to upper bound constraints of 2.5, 3.5, and 4.0 Å, respectively. The asterisks indicate potential NOE connectivities that could not be obtained due to resonance overlap.

1.13 ± 0.53 Å for EMP-AF-COO$^-$. In the case of EMP-AF-NH$_2$, the rmsd drops to 0.10 ± 0.02 Å between residues 3 and 14. As for EMP-AF-COO$^-$, between residues 3 and 8, the rmsd is 0.09 ± 0.03 Å, while it varies between 0.25 ± 0.11 and 0.6 ± 0.27 Å when residues 9–14 are considered. The majority of the ϕ and ψ angles are in the most favored or additionally allowed region of the Ramachandran plot, overall indicating that the quality of the structures is quite satisfactory. In addition, panels a and b of Figure 4 show that this peptide also forms an amphipathic α-helix.

MD Simulations and ED Analysis. Since we aimed to disclose the molecular mechanism responsible for the increased flexibility of EMP-AF-COO$^-$ and because we determined experimentally the equilibrium solution structure of the two peptides in a 30:70 TFE/H$_2$O mixture (v/v), we choose to perform a 5 ns MD simulation for each peptide in an explicit solvent simulating that environment. The target was to detect the conversion of the rigid C-terminal helical

region into a more flexible one and thus to be able to pin down the factors producing such a conformational transition (*51*). Thus, we started with EMP-AF-NH$_2$ and EMP-AF-COO$^-$ folded in a full ideal α-helix. The root-mean-square fluctuation (rmsf) of the backbone atoms of the two peptides (Figure 5) was calculated over the last 2 ns of the MD simulation, where an equilibrium state was reached. The results clearly show that, in agreement with the experimental results, while the N-terminal region of the peptides exhibits comparable behavior, there is an increased level of fluctuation of the backbone atomic positions in the C-terminal region of EMP-AF-COO$^-$ after residue 9.

To disclose the specific intramolecular interactions responsible for these diverse conformational dynamics, we analyzed the behavior of the H-bonds involved in the stabilization of the α-helix secondary structure. Figure 6 shows the result of this analysis for the two peptides. As for EMP-AF-COO$^-$ (Figure 6a, top panel), the repulsive interaction between Leu14 COO$^-$ and Ile11 CO turns out to affect the stability of the Ile10 CO–Leu14 NH H-bond that is part of the α-helix H-bond network (Figure 6a, bottom panel). Interestingly, this H-bond reaches an equilibrium state after 2 ns, oscillating at ~4 Å, thus suggesting it must be unstable. Differently, in the case of EMP-AF-NH$_2$ (Figure 6b), the distance between the C-terminus amide NH$_2$ group (Leu14 NH$_2$) and the backbone carbonyl of Ile11 (Ile11 CO) (Figure 6b, top panel) and the distance between the backbone carbonyl of Ile10 (Ile10 CO) and the backbone amide of Leu14 (Leu14 NH) (Figure 6b, bottom panel) do not vary throughout the MD simulation, thus being compatible with the formation of stable H-bonds.

To understand in more detail the dynamic features of the two peptides, we carried out an ED analysis of the trajectories produced during those last 2 ns. Figure 7a shows the plot of the first 10 eigenvectors that represent the peptides' main degrees of freedom (*52*, *53*). Since the first three values account for more than 60% of the peptides' conformational fluctuations, we analyzed these three eigenvectors to obtain information about the existence of concerted displacements of some residues during the MD simulation. With respect to the eigenvalues, we did not observe a significant difference between the two peptides in their overall molecular dynamics (Figure 7a). However, the calculation of the per residue displacements along the first eigenvector of each peptide (Figure 7b) provides evidence there are some differences in their molecular dynamics. In fact, in the case of EMP-AF-NH$_2$, the principal concerted fluctuation involves mainly the first five residues, while for EMP-AF-COO$^-$, the main concerted fluctuation comprises residues in both the N- and C-termini. Overall, the ED analysis indicates that the two peptides experience concerted motions encompassing diverse regions of their primary sequence, in agreement with the existence of distinct conformational families, as evidenced by the NMR-derived structures (Figure 4). In addition, the finding that the N- and C-terminal regions of EMP-AF-COO$^-$ do not present any significant correlation of their motions explains why, for this peptide, it is not possible to identify a family of NMR-derived structures where the α-helical backbone (residues 3–14) can be superimposed as in the case of EMP-AF-NH$_2$ (Figure 4).
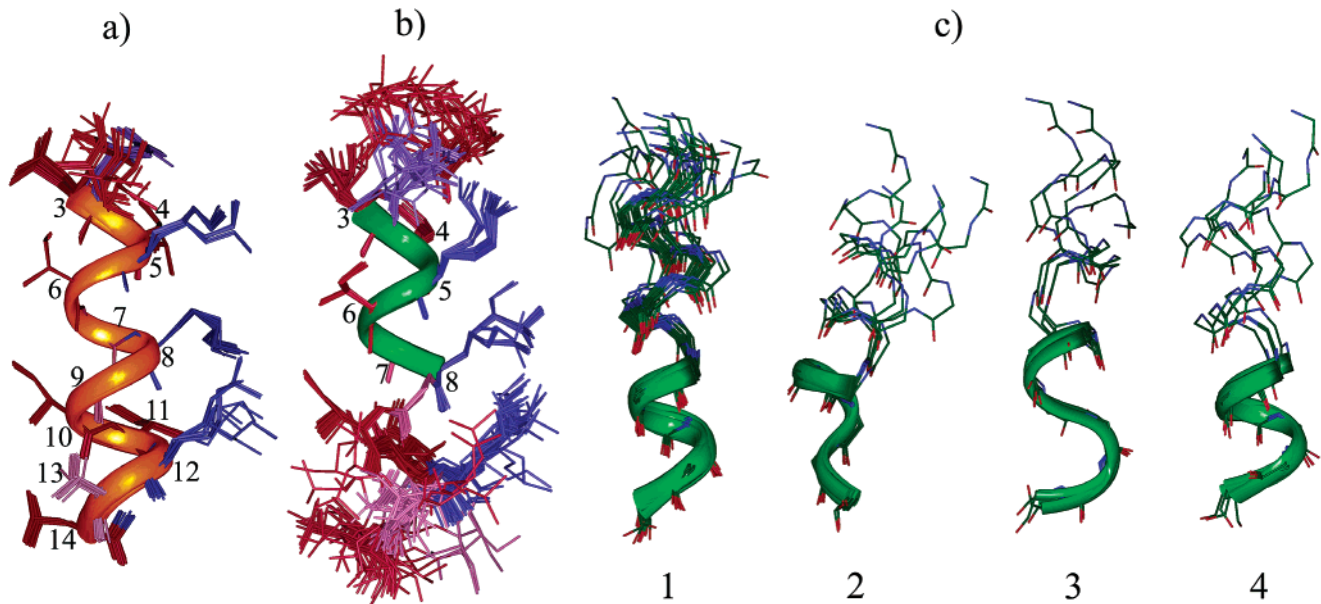
FIGURE 4: Superposition of (a) the final 20 calculated structures of EMP-AF-NH$_2$, (b) the final 35 structures of EMP-AF-COO$^-$ in a 30:70 (v/v) TFE/H$_2$O mixture at 20 °C based on the minimum pairwise rmsd of the peptide backbone spanning residues 3−14 (EMP-AF-NH$_2$) and 3−8 (EMP-AF-COO$^-$) as indicated by the ribbon, and (c) the same 35 structures of EMP-AF-COO$^-$ grouped in different conformational families according to the best superposition of residues 9−14. The hydrophobic amino acids are colored red and the charged ones blue. The C-terminus is shown at the bottom.

Table 1: Statistics for the Ensemble of 20 Structures of EMP-AF-NH$_2$ and 35 Structures of EMP-AF-COO$^-$

	EMP-AF-NH$_2$	EMP-AF-COO$^-$
no. of NOE restraints		
total distance restraints	180	210
intraresidue	102	136
sequential	42	50
medium-range	36	24
rmsd from ideal covalent geometry		
bonds (Å)	0.0037	0.0037
angles (deg)	0.5197	0.6041
impropers	0.1886	0.1994
Ramachandran plot analysis		
most favored region (%)	100	89.6
additionally allowed region (%)	0	8.8
generously allowed region (%)	0	1.0
disallowed region (%)	0	0.5
rmsd (Å)		
backbone (all)	0.26 ± 0.13	1.13 ± 0.53
backbone (residues 3−14)	0.10 ± 0.02	0.79 ± 0.51
backbone (residues 3−8)	0.07 ± 0.02	0.09 ± 0.03
heavy atoms (all)	0.55 ± 0.15	1.56 ± 0.48
heavy atoms (residues 3−14)	0.47 ± 0.12	1.36 ± 0.56
heavy atoms (residues 3−8)	0.34 ± 0.14	0.57 ± 0.15

Families of EMP-AF-COO$^-$ Superimposed between Residues 9 and 14			
family 1	family 2	family 3	family 4

	family 1	family 2	family 3	family 4
no. of structures per family	22	5	4	4
rmsd (Å)				
backbone	0.35 ± 0.11	0.25 ± 0.11	0.60 ± 0.27	0.50 ± 0.12
heavy atoms	1.04 ± 0.31	0.95 ± 0.18	1.06 ± 0.03	0.88 ± 0.08

DISCUSSION

Most of the inflammatory peptides presenting mast cell degranulating activity share common properties. In fact, they are generally composed of fewer than 60 amino acids, their net charge is positive, they are hydrophobic, and/or they present amphipathic α-helical structures (*20*). In addition, in most cases they are membrane active.

Recently, Konno and co-workers (*20*) isolated from the venom of the solitary wasp the EMP-AF-NH$_2$ peptide together with its C-terminal carboxyl-free form, both characterized by mast cell degranulating activity. They found that

EMP-AF-NH$_2$ had a 50% higher degranulating activity in rat peritoneal mast cells than EMP-AF-COO$^-$, at 10^{-5} M. Even more interestingly, they found that EMP-AF-COO$^-$ turned out to lose completely its hemolytic effect on human erythrocytes, exhibited instead by EMP-AF-NH$_2$ at 4.5 × 10^{-5} M (*20*).

Though it may occur that amidated and nonamidated forms do not differ substantially in their biological activity (*54, 55*), in a number of cases, it has been shown that the activity of the carboxyl-free form is significantly impaired (*7, 56*). Similarly, it has been reported that synthetic C-terminally
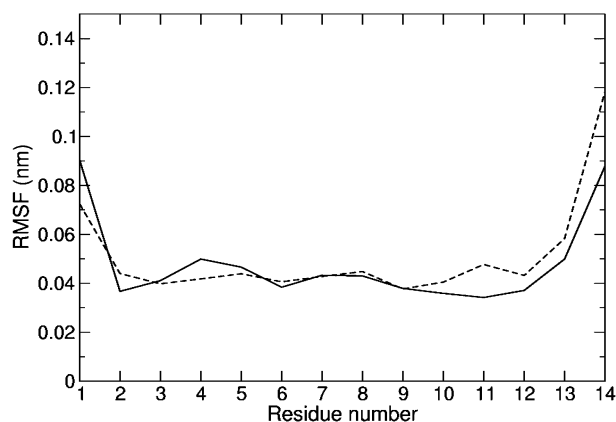
FIGURE 5: Root-mean-square fluctuation (rmsf) of EMP-AF-NH$_2$ (—) and EMP-AF-COO$^-$ (- - -) backbone atoms during the last 2 ns of each MD simulation in a 30:70 (v/v) TFE/H$_2$O mixture.

amidated analogues of peptides, whose native forms are not amidated, exhibit increased biological activity (*14−16, 57, 58*). Thus, the reduced inflammatory and antimicrobial activity of nonamidated peptides is generally ascribed to a reduced net positive charge or to a reduced helical structure.

Recently, however, Shalev et al. (*59*), while studying the consequences of carboxy amidation on dermaseptin S3, found

that the enhanced bacterial growth inhibition potency exhibited by the amidated form had to be associated with a more rigid and extended α-helical structure. One point they could not explain, though, was why amidation produces such a significant conformational change throughout most of the peptide sequence. These observations prompted us to investigate in more detail the origin of the differences in the cytolytic activity of EMP-AF-NH$_2$ and EMP-AF-COO$^-$.

Addition of negative charges at the negative pole of the α-helix macrodipole is expected to destabilize the helical structure (*15*). In fact, certainly the CD experiments indicate a lower helicity for the C-terminal carboxyl-free peptide, both in TFE and in the presence of SDS micelles (Figure 1a,b).

As has been suggested by others (*17, 23, 24*), we do believe that a crucial step that affects the efficiency with which the peptides perturb and permeabilize the membranes is associated with the conformational changes that take place just before the effective interaction with the membrane surface. Therefore, we have chosen to study the structure of the peptides in an H$_2$O/TFE mixture that is known to mimic that environment (*23, 24*).

The NMR-derived solution structures of EMP-AF-NH$_2$ and EMP-AF-COO$^-$ (Figure 4) show that while both peptides possess an amphipathic helical structure, only EMP-AF-NH$_2$
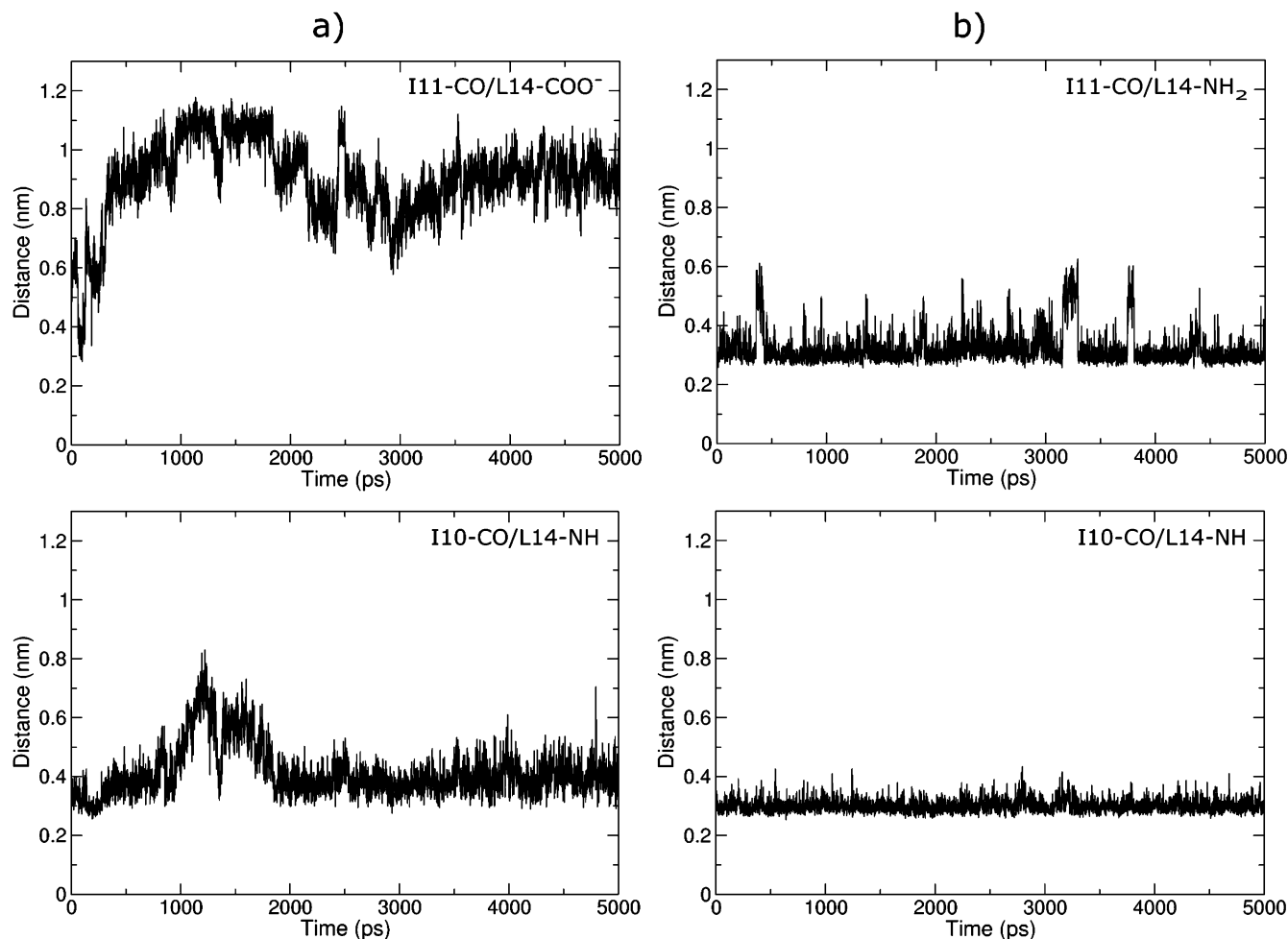

FIGURE 6: Behavior of distances between specific atoms during the MD simulations. (a) For EMP-AF-COO$^-$, distances between the backbone carbonyl group of Ile11, I11 CO, and the free carboxylate group of Leu14, L14 COO$^-$, and between the backbone carbonyl group of Ile10, I10 CO, and the backbone amide group of Leu14, L14 NH. (b) For EMP-AF-NH$_2$, distances between the backbone carbonyl group of Ile11, I11 CO, and the Leu14 C-terminus, L14 NH$_2$, and between the backbone carbonyl group of Ile10, I10 CO, and the backbone amide group of Leu14, L14 NH.
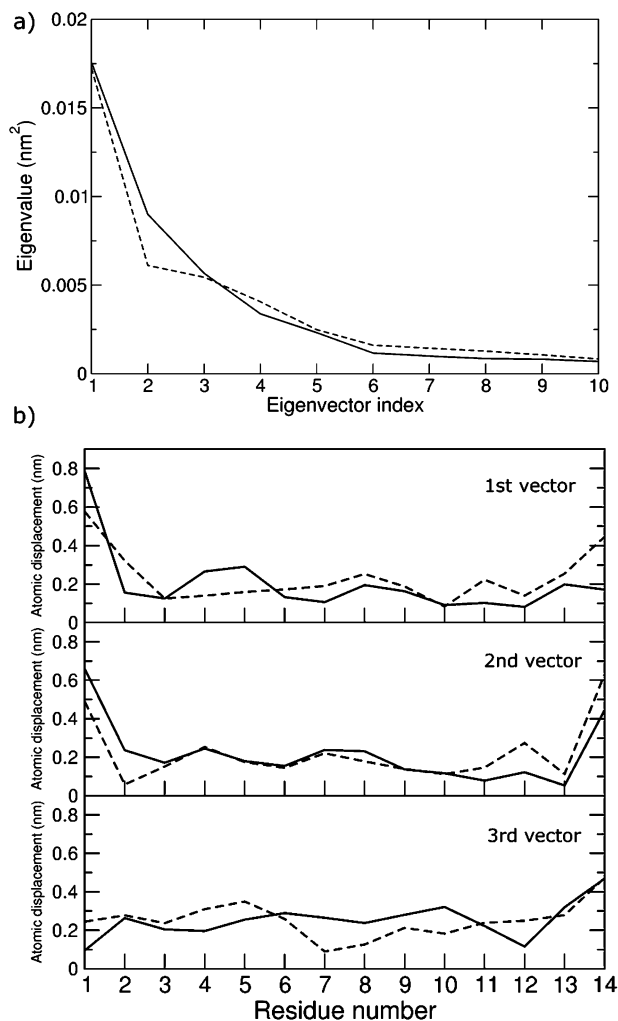
FIGURE 7: (a) Eigenvalue spectra for the last 2 ns of simulations of EMP-AF-NH$_2$ (—) and EMP-AF-COO$^-$ (- - -). (b) Atomic displacements (nanometers) along the first three eigenvectors for each trajectory.

exhibits a rigid and well-defined molecular conformation compatible with the observed higher helicity. A detailed analysis of the NMR-derived structures of EMP-AF-COO$^-$, instead, shows the existence of a number of conformational families characterized by a common helical region in the N-terminus while presenting a variety of helical stretches in the C-terminus. As has been concluded in other cases (*60*, *61*), this finding indicates that the peptide possesses a certain degree of conformational flexibility in that region.

The use of MD simulation has turned out to be quite useful in the study of the conformational changes associated with the biological activity of peptides. In recent studies on membrane active peptides, by using extensive restrained molecular dynamics simulation, in vacuum, for the lantibiotic peptide mutacin 1140 (*61*) it has been possible to demonstrate the flipping of amide protons from a solvent-protected to a solvent-exposed location. Relying on the fact that similar structural changes have been observed for nisin while switching from the membrane-bound to the unbound state, it has been inferred that this might be a structural feature common to the membrane-interacting lantibiotics.

On the basis of these results, to disclose the nature of the intramolecular interactions responsible for the diverse behavior of EMP-AF-NH$_2$ and EMP-AF-COO$^-$, we have decided to use a similar approach. In our case, however, we were interested in understanding the origin of the destabilization of the well-defined helical structure of EMP-AF-NH$_2$. For that reason, we performed 5 ns unrestrained MD simulations starting with the two peptides in an ideal α-helical conformation and immersed in an explicit solvent box mimicking the NMR experimental conditions (*51*). Overall, the simulations agree very well with the experimental data, as suggested by the rmsf behavior (Figure 5): the higher rmsf for the C-terminus of the deamidated peptide reflects the higher flexibility of that region as observed by NMR. In fact, the MD data provide novel information, at the atomic level, about the mechanism responsible for the conformational features and functional properties observed for the two peptides.

To identify the pattern through which the ideal α-helix is transformed along the MD simulation, we analyzed the hydrogen bond distances that define the α-helix conformation at the C-terminus. As shown in Figure 6b, in the EMP-AF-NH$_2$ peptide, the presence of the Ile11 CO$-$Leu14 NH$_2$ H-bond stabilizes the C-terminal region, while in EMP-AF-COO$^-$, the fact that the H-bond is substituted by the onset of a charge repulsion destabilizes the Ile10 CO$-$Leu14 NH H-bond. Such a destabilization, however, does not produce an unfolding of the helix in that region. Instead, it provides the peptide with some new degrees of conformational freedom as revealed by the NMR-derived solution structures of EMP-AF-COO$^-$ (Figure 4b,c). Recognizing that the biological activity of peptides and proteins depends not only on the presence of specific secondary structure elements but also on their concerted motion, we have used ED analysis (*62*$-$*64*) to disclose these functionally relevant dynamic features. As a result, EMP-AF-NH$_2$ can be depicted like a rigid amphipathic helix ideal for interacting efficiently with the membrane surface, as has been found for other peptides (*65*, *66*). Interestingly, as for mastoparans B and X in a TFE/H$_2$O mixture (*67*, *68*) or in a membrane-bound state (*69*), only the first two N-terminal residues experience a certain degree of flexibility, a structural feature considered relevant for the peptide biological activity (*68*). As for EMP-AF-COO$^-$, instead, the peptide structure consists of two helical segments joined at the Gly9 residue and fluctuating independently. This molecular motion generates a perturbation of the peptide hydrophobic and polar face that is expected to hamper its ability to efficiently interact with the membrane surface.

CONCLUSIONS

The enhanced potency of amidated inflammatory peptides is often attributed to their increased positive charge (*70*$-$*73*). It has been postulated that positive charges promote interactions with the predominantly negatively charged membranes and facilitate the interaction of the peptides with the cell membrane (*74*), leading to its permeabilization.

In the case of EMP-AF-COO$^-$, we have shown that, besides the expected reduction of its positive charge, the presence of the free carboxyl group at C-terminus introduces a local molecular instability that is able to partly destabilize not only the hydrogen bond pattern of that stretch of helix but the peptide as a whole. In fact, the regular amphipathic helix that in EMP-AF-NH$_2$ extends over the

entire peptide is disrupted in EMP-AF-COO⁻ by the onset of an independent fluctuation of the N- and C-terminal regions. Such structural perturbation, by amplifying its difficulty in interacting with the membrane surface, is expected to enhance the reduction of the peptide biological activity.

The fact that the CD data indicate an increase in helicity for EMP-AF-NH$_2$ on going from TFE to SDS micelles, and no differences for EMP-AF-COO⁻, strongly supports this view.

We believe this mechanistic model may help in the understanding of the relationship between the structure of inflammatory peptides and their target membranes and can be useful in devising new biologically active peptides.

ACKNOWLEDGMENT

REFERENCES

1. Banks, B. E., and Shipolini, R. A. (1986) Chemistry and pharmacology of honey-bee venom, in *Venoms of the Hymenoptera: Biochemical, Pharmacological and Behavioural Aspects* (Piek, T., Ed.) pp 327–416, Academic Press, London.
2. Nakajima, T. (1986) Pharmacological biochemistry of vespid venoms, in *Venoms of the Hymenoptera: Biochemical, Pharmacological and Behavioural Aspects* (Piek, T., Ed.) pp 309–327, Academic Press, London.
3. Konno, K., Hisada, M., Fontana, R., Lorenzi, C. C. B., Naoki, H., Itagaki, Y., Miwa, A., Kawai, N., Nakata, Y., Yasuhara, T., Neto, J. R., de Azevedo, W. F., Palma, M. S., and Nakajima, T. (2001) Anoplin, a novel antimicrobial peptide from the venom of the solitary wasp *Anoplius samariensis*, *Biochim. Biophys. Acta 1550*, 70–80.
4. Kreil, G. (1973) Biosynthesis of melittin, a toxic peptide from bee venom. Amino-acid sequence of the precursor, *Eur. J. Biochem. 33*, 558–566.
5. Andreu, D., Merrifield, R. B., Steiner, H., and Boman, H. G. (1983) Solid-phase synthesis of cecropin A and related peptides, *Proc. Natl. Acad. Sci. U.S.A. 80*, 6475–6479.
6. Mor, A., Nguyen, V. H., Delfour, A., Migliore-Samour, D., and Nicolas, P. (1991) Isolation, amino acid sequence and synthesis of dermaseptin, a novel antimicrobial peptide of amphibian skin, *Biochemistry 30*, 8824–8830.
7. Kuchler, K., Kreil, G., and Sures, I. (1989) The genes for the frog skin peptides GLa, xenopsin, levitide and caerulein contain a homologous export exon encoding a signal sequence and part of an amphiphilic peptide, *Eur. J. Biochem. 179*, 281–285.
8. Lee, I. H., Cho, Y., and Lehrer, R. I. (1997) Effects of pH and salinity on the antimicrobial properties of clavanins, *Infect. Immun. 65*, 2898–2903.
9. Agerberth, B., Lee, J.-Y., Bergman, T., Carlquist, M., Boman, H. G., Mutt, V., and Jörnvall, H. (1991) Amino acid sequence of PR-39. Isolation from pig intestine of a new member of the family of proline-arginine-rich antibacterial peptides, *Eur. J. Biochem. 2002*, 849–854.
10. Castells, P., Ampe, C., Jacobs, F., Vaeck, M., and Tempst, P. (1989) Apidaecins: antibacterial peptides from honeybees, *EMBO J. 8*, 2387–2391.
11. Harwig, S. L. S., Kokryakov, V. N., Swiderek, K. M., Aleshina, G. M., Zhao, C., and Lehrer, R. I. (1995) Prophenin-1, an exceptionally proline-rich antimicrobial peptide from porcine leukocytes, *FEBS Lett. 362*, 65–69.
12. Miyata, T., Tokunaga, F., Yoneya, T., Yoshikawa, K., Iwanaga, S., Niwa, M., Takao, T., and Shimonishi, Y. (1989) Antimicrobial peptides, isolated from horseshoe crab hemocytes, tachyplesin II, and polyphemusins I and II. Chemical structures and biological activity, *J. Biochem. 106*, 663–668.
13. Destoumieux, D., Bulet, P., Loew, D., Van Dorsselaer, A., Rodríguez, J., and Bachère, E. (1997) A new family of antimicrobial peptides in the shrimp *Penaeus vannamei* (Decapoda), *J. Biol. Chem. 272*, 28398–28406.
14. Sandvik, A. K., and Dockray, G. J. (1999) Biological activity of carboxy-terminal gastrin analogs, *Eur. J. Pharmacol. 364*, 199–203.
15. Katayama, H., Ohira, T., Aida, K., and Nagasawa, H. (2002) Significance of a carboxyl-terminal amide moiety in the folding and biological activity of crustacean hyperglycemic hormone, *Peptides 23*, 1537–1546.
16. Ali, M. F., Soto, A. M., Knoop, F. C., and Conlon, J. M. (2001) Antimicrobial peptides isolated from skin secretions of the diploid frog, *Xenopus tropicalis* (Pipidae), *Biochim. Biophys. Acta 1550*, 81–89.
17. Shai, Y. (1999) Mechanism of the binding, insertion and destabilization of phospholipid bilayers membranes by α-helical antimicrobial and cell non-selective lytic peptides, *Biochim. Biophys. Acta 1462*, 55–70.
18. Shai, Y. (2002) Mode of action of membrane active antimicrobial peptides, *Biopolymers 66*, 236–248.
19. van't Hof, W., Verrman, E. C. I., Helmerhorst, E. J., and Amerongen, A. V. N. (2001) Antimicrobial peptides: properties and applicability, *Biol. Chem. 382*, 597–619.
20. Konno, K., Hisada, M., Naoki, H., Itagaki, Y., Kawai, A., Miwa, A., Yasuhara, T., Morimoto, Y., and Nakata, Y. (2000) Structure and biological activity of eunamine mastoparan-AF (EMP-AF), a new mast cell degranulating peptide in the venom of the solitary wasp (*Anterhynchium flavomarginatum micado*), *Toxicon 38*, 1505–1515.
21. Canduri, F., Delatorre, P., Fadel, V., Lorenzi, C. C. B., Pereira, J. H., Olivieri, J. R., Neto, J. R., Konno, K., Palma, M. S., Yamane, T., and de Azevedo, W. F. (2000) Crystallization and preliminary X-ray diffraction analysis of a eumenine mastoparan toxin: a new class of mast-cell degranulating peptide in the wasp venom, *Acta Crystallogr. D56*, 1434–1436.
22. Delatorre, P., Olivieri, J. R., Neto, J. R., Lorenzi, C. C. B., Canduri, F., Fadel, V., Konno, K., Palma, M. S., Yamane, T., and de Azevedo, W. F. (2001) Preliminary cryocrystallography analysis of an eumenine mastoparan toxin isolated from the venom of the wasp *Anterhynchium flavomarginatum micado*, *Biochim. Biophys. Acta 1545*, 372–376.
23. Oren, Z., and Shai, Y. (1997) Selective lysis of bacteria but non mammalian cells by diastereomers of mellitin: Structure–function study, *Biochemistry 36*, 1826–1835.
24. Kustanovich, I., Shalev, D. E., Mikhlin, M., Gaidukov, L., and Mor, A. (2002) Structural requirements for potent versus selective cytotoxicity for antimicrobial dermaseptin S4 derivatives, *J. Biol. Chem. 277*, 16941–16951.
25. Hirota, N., Mizuno, K., and Goto, Y. (1998) Group additive contributions to the alcohol-induced α-helix formation of melittin: implication for the mechanism of the alcohol effects on proteins, *J. Mol. Biol. 275*, 365–378.
26. Sonnichsen, F. D., Van Eyk, J. E., Hodges, R. S., and Sykes, B. D. (1992) Effect of trifluoroethanol on protein secondary structure: an NMR and CD study using a synthetic actin peptide, *Biochemistry 31*, 8790–8798.
27. Chen, Y. H., Yang, J. T., and Chau, K. H. (1974) Determination of the helix and β form of proteins in aqueous solution by circular dichroism, *Biochemistry 13*, 3350–3359.
28. Piantini, U., Sorensen, O. W., Bodenhausen, G., and Ernest, R. R. (1982) Multiple quantum filters for elucidating NMR coupling networks, *J. Am. Chem. Soc. 104*, 6800–6801.
29. Braunschweiler, L., and Ernest, R. R. (1983) Coherence transfer by isotropic mixing: application to proton correlation spectroscopy, *J. Magn. Reson. 53*, 521–528.
30. Kumar, A., Ernst, R. R., and Wüthrich, K. (1980) A two-dimensional nuclear Overhauser enhancement (2D NOE) experiment for the elucidation of complete proton–proton cross-relaxation networks in biological macromolecules, *Biochem. Biophys. Res. Commun. 95*, 1–6.
31. Macura, S., and Ernst, R. R. (1980) Elucidation of cross relaxation in liquids by two-dimensional NMR spectroscopy, *Mol. Phys. 41*, 95–117.
32. States, D. J., Haberkorn, R. A., and Ruben, D. J. (1982) A Two-Dimensional Nuclear Overhauser Experiment with Pure Absorption Phase in Four Quadrants, *J. Magn. Reson. 48*, 286–292.
33. Delaglio, F., Grzesiek, S., Vuister, G. W., Zhu, G., Pfeifer, J., and Bax, A. (1995) NMRPipe: a multidimensional spectral processing system based on UNIX pipes, *J. Biomol. NMR 6*, 277–293.

34. Johnson, B., and Blevins, R. A. (1994) NMRView: A computer program for the visualization and analysis of NMR data, *J. Biomol. NMR 4*, 603−614.

35. Güntert, P., Mumenthaler, C., and Wüthrich, K. (1997) Torsion Angle Dynamics for NMR Structure Calculation with the New Program Dyana, *J. Mol. Biol. 273*, 283−298.

36. Pristovšek, P., Rüterjans, H., and Jerala, R. (2002) Semiautomatic sequence-specific assignment of proteins based on the tertiary structure: The program st2 NMR, *J. Comput. Chem. 23*, 335−340.

37. Dauber-Osguthorpe, P., Osguthorpe, V. A., Wolff, D. J., Genest, M., and Hagler, A. T. (1988) Structure and energetics of ligand binding to proteins: *E. coli* dihydrofolate reductase-trimethoprim, a drug-receptor system, *Proteins: Struct., Funct., Genet. 4*, 31−47.

38. *INSIGHT II User Guide*, version 95 (1995) Accelrys Inc., San Diego.

39. Laskowsky, R. A., Rullmann, J. A., MacArthur, M. W., Kaptein, R., and Thorton, J. M. (1996) AQUA and PROCHECK-NMR: programs for checking the quality of protein structures solved by NMR, *J. Biomol. NMR 8*, 477−486.

40. Brunger, A. T., Adams, P. D., Clore, G. M., Delano, W. L., Gros, P., Grosse-Kunstleve, R. W., Jiang, J.-S., Kuszewski, J., Nilges, N., Pannu, N. S., Read, R. J., Rice, L. M., Simonson, T., and Warren, G. L. (1998) Crystallography and NMR system (CNS): a new software system for macromolecular structure determination, *Acta Crystallogr. D54*, 905−921.

41. Lindahl, E., Hess, B., and van der Spoel, D. (2001) Gromacs 3.0: a package for molecular simulation and trajectory analysis, *J. Mol. Model. 7*, 306−317.

42. Berendsen, H. J. C., Postma, J. P. M., van Gunsteren, W. F., and Hermans, J. (1981) Interaction models for water in relation to protein hydration, in *Intermolecular Forces* (Pullman, B., Ed.) pp 331−342, Reidel Publishing Co., Dordrecht, The Netherlands.

43. Fioroni, M., Burger, K., Mark, A. E., and Roccatano, D. (2000) A new 2,2,2-trifluoroethanol model for molecular dynamics simulations, *J. Phys. Chem. B 104*, 12347−12354.

44. Darden, T., York, D., and Pedersen, L. (1993) Particle Mesh Ewald: An N-log(N) method for Ewald sums in large systems, *J. Chem. Phys. 98*, 10089−10092.

45. Cheatham, T. E., III, Miller, J. L., Fox, T., Darden, T. A., and Kollman, P. A. (1995) Molecular dynamics simulations on solvated biomolecular systems: The Particle Mesh Ewald method leads to stable trajectories of DNA, RNA, and proteins, *J. Am. Chem. Soc. 117*, 4193−4194.

46. Hess, B., Bekker, H., Berendsen, H. J. C., and Fraaije, J. G. E. M. (1997) LINCS: A linear constraint solver for molecular simulations, *J. Comput. Chem. 18*, 1463−1472.

47. Miyamoto, S., and Kollman, P. A. (1992) SETTLE: An analytical version of the SHAKE and RATTLE algorithm for rigid water models, *J. Comput. Chem. 13*, 952−962.

48. van Aalten, D. M. F., de Groot, B. L., Findlay, J. B. C., Berendsen, H. J. C., and Amadei, A. (1997) A comparison of techniques for calculating protein essential dynamics, *J. Comput. Chem. 18*, 169−181.

49. Wüthrich, K. (1986) *NMR of Proteins and Nucleic Acids*, John Wiley & Sons, New York.

50. Wishart, D. S., Sykes, B. D., and Richards, F. M. (1992) The Chemical Shift Index: A fast and simple method for the assignment of protein secondary structure through NMR spectroscopy, *Biochemistry 31*, 1647−1651.

51. Levy, Y., Hanan, E., Solomon, B., and Becker, O. M. (2001) Helx-coil transition of Pr106−126: Molecular dynamic study, *Proteins: Struct., Funct., Genet. 45*, 382−396.

52. Amadei, A., Linssen, A. B. M., and Berendsen, H. J. C. (1993) Essential dynamics of proteins, *Proteins: Struct., Funct., Genet. 17*, 412−425.

53. de Groot, B. L., van Aalten, D. M. F., Amadei, A., and Berendsen, H. J. C. (1996) The consistency of large concerted motions in proteins in molecular dynamics simulations, *Biophys. J. 71*, 1707−1713.

54. Lee, I. H., Zhao, C., Cho, Y., Harwig, S. S., Cooper, E. L., and Lehrer, R. I. (1997) Clavanins, α-helical antimicrobial peptides from tunicate hemocytes, *FEBS Lett. 400*, 158−162.

55. Yasin, B., Lehrer, R. I., Harwig, S. S., and Wagar, E. A. (1996) Protegrins: structural requirements for inactivating elementary bodies of *Chlamydia trachomatis*, *Infect. Immun. 64*, 4863−4866.

56. Nakajima, Y., Qu, X.-M., and Natori, S. (1987) Interaction between liposomes and sarcotoxin IA, a potent antibacterial protein of *Sarcophaga peregrina* (flesh fly), *J. Biol. Chem. 262*, 1665−1669.

57. Mor, A., and Nicolas, P. J. (1994) The NH2-terminal α-helical domain 1−18 of dermaseptin is responsible for antimicrobial activity, *J. Biol. Chem. 269*, 1934−1939.

58. Fernández, R. C., and Weiss, A. A. (1996) Susceptibilities of *Bordetella pertussis* strains to antimicrobial peptides, *Antimicrob. Agents Chemother. 40*, 1041−1043.

59. Shalev, D. E., Mor, A., and Kustanovich, I. (2002) Structural consequences of carboxyamidation of dermaseptin S3, *Biochemistry 41*, 7312−7317.

60. de Chiara, C., Nicastro, G., Spisni, A., Zanotti, F., Cocco, T., and Papa, S. (2002) Activity and NMR structure of synthetic peptides of the bovine ATPase inhibitor protein, IF1, *Peptides 23*, 2127−2141.

61. Smith, L., Zachariah, C., Thirumoorthy, R., Rocca, J., Novák, J., Hillman, J. D., and Edison, A. S. (2003) Structure and dynamics of the lantbiotic mutacin 1140, *Biochemistry 42*, 10372−10384.

62. van Aalten, D. M. F., Findlay, J. B. C., Amadei, A., and Berendsen, H. J. C (1995) Essential dynamics of the cellular retinol-binding protein: Evidence for ligand induced conformational changes, *Protein Eng. 8*, 1129−1135.

63. de Groot, B. L., Daura, X., Mark, A. E., and Grubmüller, H. (2001) Essential dynamics of reversible peptide folding: Memory-free conformational dynamics governed by internal hydrogen bonds, *J. Mol. Biol. 309*, 299−313.

64. Grottesi, A., and Sansom, M. S. (2003) Molecular dynamics simulations of a K+ channel blocker: Tc1 toxin from *Tityus cambridgei*, *FEBS Lett. 535*, 29−33.

65. Simmaco, M., Mignona, G., and Barra, D. (1998) Antimicrobial peptides from amphibian skin: What do they tell us? *Biopolymers 47*, 435−450.

66. Prates, M. V., Sforça, M. L., Regis, W. C. B., Leite, J. R. S. A., Silva, L. P., Pertinhez, T. A., Araújo, A. L. T., Azevedo, R. B., Spisni, A., and Bloch, C., Jr. (2004) The NMR-derived solution structure of a new cationic antimicrobial peptide from the skin secretion of the anuran *Hyla punctata*, *J. Biol. Chem. 279*, 13018−13026.

67. Chuang, C.-C., Huang, W.-C., Yu, H.-M., Wang, K.-T., and Wu, S.-H. (1996) Conformation of *Vespa basalis* Mastoparan-B in trifluoroethanol-containing aqueous solution, *Biochim. Biophys. Acta 1292*, 1−8.

68. Ho, C. L., Lin, Y. L., Chen, L. L., Hwang, H., Yu, M., and Wang, K. T. (1996) Structural requirements for the edema-inducing and haemolytic activities of mastoparan B isolated from the hornet (*Vespa basalis*) venom, *Toxicon 34*, 1027−1035.

69. Wakamatsu, K., Okada, A., Miyazawa, T., Ohya, M., and Higashijima, T. (1992) Membrane-bound confirmation of mastoparan-X, a G-protein-activating peptide, *Biochemistry 31*, 5654−5660.

70. Pouny, Y., Rapaport, D., Mor, A., Nicolas, P., and Shai, Y. (1992) Interactions of antimicrobial dermaseptin and its fluorescently labeled analogues with phospholipid membranes, *Biochemistry 31*, 12416−12423.

71. Cociancich, S., Ghazi, A., Hetru, C., Hoffmann, J. A., and Letellier, L. (1993) Insect defensin, an inducible antibacterial peptide, forms voltage-dependent channels in *Micrococcus luteus*, *J. Biol. Chem. 268*, 19239−19245.

72. Ludtke, S., He, K., and Huang, H. (1995) Antimicrobial peptide pores in membranes detected by neutron in-plane scattering, *Biochemistry 34*, 16764−16769.

73. Steiner, H., Andreu, D., and Merrifield, R. B. (1988) Binding and action of cecropin and cecropin analogues: antibacterial peptides from insects, *Biochim. Biophys. Acta 939*, 260−266.

74. Tossi, A., Sandri, L., and Giangaspero, A. (2000) Amphipathic, α-helical antimicrobial peptides, *Biopolymers 55*, 4−30.